

Separation of Benzoic and Unconjugated Acidic Components of Leonardite Humic Material Using Sequential Solid-Phase Extraction at Different pH Values as Revealed by Fourier Transform Ion Cyclotron Resonance Mass Spectrometry and Correlation Nuclear Magnetic Resonance Spectroscopy

Alexander Zherebkov,^{†,‡,§,¶} Evgeny Shirshin,^{||} Oleg Kharybin,^{†,§} Yury Kostyukovich,^{†,§,#,○} Alexey Kononikhin,^{§,‡,#} Andrey I. Konstantinov,[‡] Dmitry Volkov,[‡] Vitaliy A. Roznyatovsky,[‡] Yuri K. Grishin,[‡] Irina V. Perminova,^{*‡,¶} and Eugene Nikolaev^{*†,§,‡,#}

[†] Skolkovo Institute of Science and Technology, 143025 Skolkovo, Moscow Region, Russia

[‡] Department of Chemistry, Lomonosov Moscow State University, 119991 Moscow, Russia

[§] Institute for Energy Problems of Chemical Physics of Russian Academy of Sciences, Leninskij Prospekt 38-2, 119334 Moscow, Russia

^{||} Department of Physics, Lomonosov Moscow State University, Leninskie Gory 1/2, 119991 Moscow, Russia

^{*} Orehovich Institute of Biomedical Chemistry, Russian Academy of Sciences, Pogodinskaya Ulitsa 10, 119121 Moscow, Russia

[#] Moscow Institute of Physics and Technology, 141700 Dolgoprudnyi, Moscow Region, Russia

Supporting Information

ABSTRACT: Here, we report on sequential solid-phase extraction of leonardite humatominic acid (CHM) on a non-ionic sorbent at four steadily lowered pH values: 7, 5, 3, and 2, yielding fractions with different acidic properties. Using nuclear magnetic resonance (NMR) spectroscopy and ultrahigh-resolution mass spectrometry, we revealed a gradual shift of dominating scaffolds in the fractions of CHM from reduced saturated to oxidized aromatic compounds. An increase on the average aromaticity of the CHM fractions was accompanied by a red shift in fluorescence spectra. These results were supported by heteronuclear single quantum coherence and heteronuclear multiple bond correlation NMR experiments. We have demonstrated that the CHM fraction isolated at pH 5 was dominated by aliphatic carboxyl carriers, while the pH 3 fraction was dominated by aromatic carboxyl acids. The developed fractionation technique will enable deeper insight on structure–property relationships and the design of the humic-based materials with tailored reactive properties.

KEYWORDS: fractionation, leonardite, humic substances, structure, FTICR MS, extraction

1. INTRODUCTION

Humic substances (HS) are the products of microbial and abiotic oxidation of remnants of living organisms. They are ubiquitous in the environment and constitute the major fraction of the caustoboliths, e.g., coal, leonardite, peat, and oil shale.¹ Unlike petroleum, which consists mostly of hydrocarbons and aromatic heterocycles, leonardite HS are enriched with oxygen-containing compounds carrying carboxylic and phenolic groups,² which are arranged into a supramolecular ensemble.³ The acidic character of HS is responsible for their ability to bind heavy metals, which is important for soil remediation.⁴ Binding properties of HS are of particular importance for agricultural applications,⁵ where they are used for plant nutrition in the form of water-soluble complexes with microelements.⁶ Recently, a lot of attention was paid to the reported increase in bioavailability of iron-based nanomaterials stabilized by leonardite-derived HS.⁷ However, extreme molecular heterogeneity hinders systematic characterization of metal binding with HS. Even the most powerful analytical techniques require preliminary fractionation of HS to obtain

structural information on their major moieties.⁸ This boosts research on isolation and characterization of the distinct constituents of HS to obtain a fraction with the tailored properties,⁹ e.g., with enhanced complexation capacity with regard to iron.

Common separation of HS using changes in the pH value and ionic strength yields fractions with a similar molecular mass distribution¹⁰ but with different contents of aliphatic structural moieties (gray humic acid) and aromatic structural fragments (brown humic acid).¹¹ Sequential solvent extraction with a polarity gradient was applied for crude oils and petroleum refinery byproducts.¹² For HS, fractionation with regard to polarity and carboxyl group content was facilitated on non-ionic macroporous resins. Application of sequential extraction on the Amberlite XAD-4 and XAD-8 resins enabled

Received: July 30, 2018

Revised: October 4, 2018

Accepted: October 18, 2018

Published: October 18, 2018

separation of “hydrophobic” and “hydrophilic” fractions, which differed in contribution of aromatic carbon and carboxyls.¹³

Deeper fractionation of HS was achieved by application of gradient elution from XAD-8.¹⁴ A stepwise elution of soil HS was conducted by buffer solution adjusted to pH 7 and 11, followed by a 50% water–ethanol mixture. It yielded fractions differing in acidic group content and the H/C and O/C atomic ratios.¹⁴ The pronounced differences were observed for a fraction eluted at pH 7 and for an alcohol eluate: they were characterized by a dominant contribution of aromatic and aliphatic fragments, respectively. The linear pH-gradient elution was also applied for column fractionation of both soil and water HS,¹⁵ and their model compounds differing in acidity: phenol, benzoic acid, and vanillin.¹⁶ It was found that the retention pH correlated with the pK_a value of the model compounds. Similar results were also achieved in the case of HS.

Introduction of Fourier transform ion cyclotron resonance mass spectrometry (FTICR MS) with soft ionization techniques facilitated exploration of the molecular profiles of HS.¹⁷ However, the XAD-based fractionation techniques were hardly compatible with FTICR MS requirements because of the buffer usage, which suppresses the ionization of organic compounds in negative-ion mode.¹⁸ An effective solution of this problem was an application of chromatography with organic–water eluents. Separation of Suwannee River dissolved organic matter (DOM) by hydrophilic interaction chromatography (HILIC) showed uneven distribution of key substructures across the 80 fractions.¹⁹ Cyclic and linear terpenoids were prominent in the most hydrophobic fractions, whereas hydrophilic fractions showed an abundance of carbohydrates and aromatic amino acids. The FTICR MS study of three fractions of the Suwannee River fulvic acid (SRFA) obtained by reversed-phase high-performance liquid chromatography (RP HPLC) showed the gradual shift in their molecular compositions.²⁰ This was demonstrated by plotting the FTICR MS data in Van Krevelen diagrams (relationship of the H/C versus O/C ratio). The authors have shown that the first most hydrophilic eluate consisted mostly of polycarboxylic compounds. A common disadvantage of these approaches is a lack of scaling possibilities for obtaining large quantities of fractionated materials, which are needed for field experiments.

In our previous work, we have demonstrated that fractions of HS from different sources, including leonardite, displayed similar distributions of carboxyl-carrying constituents over the Van Krevelen diagram, which were characterized by a gradual shift from lignins, condensed tannins, and carbohydrates to carboxylic-rich unsaturated oxygenated compounds.^{21,22} The observed patterns suggested the feasibility of preparative separation of HS using differences in pK_a values of their acidic constituents: phenols, aliphatic acids, aromatic carboxylic acids, and ketoacids. This allowed us to propose a new separation method for leonardite humic material based on the use of sequential extraction at different pH values on the modified styrene divinylbenzene resin (Bond Elut PPL cartridge). Molecular compositions of the separated fractions were analyzed using FTICR MS, nuclear magnetic resonance (NMR) spectroscopy, and fluorescence spectroscopy.

2. MATERIALS AND METHODS

2.1. Materials and Reagents. Leonardite hymatomelanic acid (CHM) was used as a parent humic material. It was isolated by exhaustive ethanol extraction in a Soxhlet apparatus of freshly

precipitated humic acids obtained by acidification of potassium humate (“Gumat-80”, Irkutsk, Russia). Refluxing and filtration of the insoluble part were repeated 3 times. The characteristics of the obtained product are given in our previous publication.²³ Solvents and other reagents used in this study were of analytical grade. Ethanol and methanol for HPLC (Lab-Scan) were used for elution and dissolution. High-purity distilled water was prepared using a Millipore Simplicity 185 water purifying system. Bond Elut PPL (Agilent Technologies) cartridges (5 g, 60 mL) were used for isolation of CHM fractions.

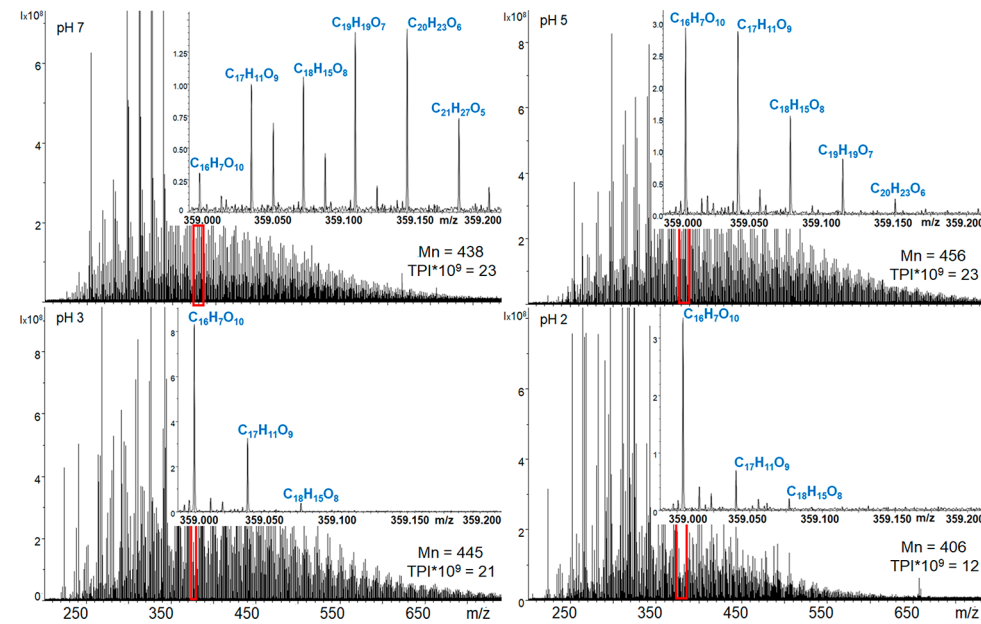
2.2. pH-Gradient Separation of the Humic Material under Study Using Bond Elut PPL Cartridges. The sequential separation of the CHM material was conducted on the PPL cartridges using four subsequent extractions at different pH values: 7, 5, 3, and 2. The cartridge treatment and extraction protocols were as described by Dittmar et al.²⁴ In brief, a volume of 600 mL of CHM solution (0.5 g/L) was adjusted to pH 7 and passed through the activated cartridge. The output solution was collected and used for the follow-up fractionation by adjusting pH to 5 and discharging it through the second PPL cartridge. The same procedure was repeated with adjusting pH to 3 and finally to 2. Prior to extraction, each cartridge was activated by methanol and equilibrated with solution at the working pH using HCl. The isolated CHM fractions were assigned the indexes with the corresponding pH value (e.g., CHM-7 for pH 7). A scheme of the extraction procedure is presented in Figure S1 of the Supporting Information. The fraction yields were 56 mg (19%), 28 mg (9%), 34 mg (11%), and 22 mg (7%) for CHM-7, CHM-5, CHM-3, and CHM-2, respectively. Each of the recovered fractions was analyzed by FTICR MS, NMR spectroscopy, and fluorescence spectroscopy.

2.3. FTICR MS. All experiments were performed on FTICR MS Bruker Apex Ultra with a harmonized cell²⁵ equipped with a 7 T superconducting magnet and electrospray ionization (ESI) source. Prior to analysis, all HS samples were diluted with methanol to 100 mg/L and then injected into the ESI source using a microliter pump at a flow rate of 90 μ L/h with a nebulizer gas pressure of 138 kPa and a drying gas pressure of 103 kPa. A source heater was kept at 200 °C to ensure rapid desolvation in the ESI droplets. Mass spectra were first externally calibrated using an in-house made carboxylated polystyrene standard.²⁶ Internal calibration was systematically performed using the known peak series of natural organic matter (NOM), reaching accuracy values of <0.2 ppm. The spectra were acquired within a time domain of 4 Megawords in ESI(−), and 300 scans were accumulated for each spectrum. Resolving power was 530 000 at m/z 400. The FTICR MS data were processed using the lab-made “Transhumus” software designed by Grigoriev, which is based on the total mass difference statistics algorithm.²⁷ The generated CHONS formulas were validated by setting sensible chemical constraints [O/C ratio, ≤1; H/C ratio, ≤2; element counts (C, ≤120; H, ≤200; O, ≤60; N, ≤2; and S, ≤1); and mass accuracy window, <1 ppm]. The assigned CHNOS formulas were further plotted in the Van Krevelen diagrams.²⁸

2.4. NMR Spectroscopy. The structural group composition of the CHM fractions was determined using solution-state ^{13}C NMR spectroscopy. All fractions (about 30 mg) were dissolved in 0.6 mL of 0.3 M NaOD/D₂O, except for CHM-3, which was dissolved in DMSO-*d*₆. The ^{13}C NMR spectra were recorded on a Bruker Avance-400 spectrometer operating at 100 MHz for carbon nuclei using a Carr–Purcell–Meiboom–Gill (CPMG) sequence with an initial 90° pulse; the registration time of the free induction decay was 0.2 s, and the relaxation delay between the pulses was 7.8 s.²⁹ The recorded flame ionization detector (FID) signals were multiplied by the exponent with a spectral line broadening (lb) parameter of 100 Hz before Fourier transformation. The processing and transformation of the spectra were performed using the MestReC software package. The integration was performed using the following assignments: 220–187 ppm for carbonyl groups, 187–165 ppm for carboxyl, ester, and amide groups, 165–145 ppm for substituted aromatic fragments, 145–108 ppm for unsubstituted aromatic fragments, 108–48 ppm for

Table 1. Normalized ^{13}C NMR Integrals and Typical HS Substructures²⁹

range (ppm)	carbon distribution (%)						
	CH _n	CH ₃ O	CH ₂ O + CHO	OCO	C _{ar} + C _{ar} O	COO	C=O
0–48	48–55	55–89	89–112	112–164	164–187	187–220	
parent CHM	15	4	5	3	56	15	6
CHM-7	24	3	7	5	44	13	3
CHM-5	16	4	10	7	50	11	4
CHM-3	13	2	8	4	48	16	9
CHM-2	13	4	6	5	45	16	11

**Figure 1.** FTICR mass spectra of the PPL fractions of the parent CHM material obtained by subsequent lowering of the pH value of the discharging solutions following the trend in the corresponding pK_a values of phenols, unconjugated carboxylic acids and ketoacids.

heteroatom-substituted aliphatic fragments, and 48–5 ppm for aliphatic chains (Table 1).²⁹

The gHSQC and gHMBC two-dimensional (2D) NMR spectra of CHM-3 and CHM-5 were acquired using the Agilent 400MR spectrometer (400.0 and 100.6 MHz resonance frequency for ^1H and ^{13}C , respectively). The measurement times of gHSQC experiments (150 scans per t_1 increment, 128 t_1 increments, and $^1\text{J}_{\text{CH}}$ of 146 Hz) were about 13 h and about 23 h for gHMBC experiments (260 scans per t_1 increment, 128 t_1 increments, and $^2\text{J}_{\text{CH}}$ of 8 Hz).

The integration of ^1H NMR spectra was conducted using the following assignments: 0–2.05 ppm, aliphatic protons (CH_n protons); 2.05–3.2 ppm, α protons ($\text{X}-\text{CH}_\omega$, where X is COOH, COOR, C_{ar}, etc.); 3.2–4.5 ppm, protons in functional groups [$\text{C}-\text{X}-\text{H}$, where X is O, N, O(N)H]; 4.5–6.5 ppm, alkenes and alkynes; and 6.5–10.0 ppm, aromatic and phenolic protons (C_{ar}H and C_{ar}OH). The spectral intensity of residual H atoms of DMSO- d_6 at 2.5 ppm was subtracted from the spectral integral of α -CH protons.

2.5. Fluorescence Measurements. Fluorescence spectra were recorded using the FluoroMax-4 fluorometer (Horiba Horiba Yvon). Excitation–emission matrixes (EEMs) were measured; the excitation wavelength varied in the range from 280 to 420 nm, while the emission was detected from 300 to 700 nm. The excitation and emission slit widths were set to 5 nm, and the correction of spectra to the excitation intensity was performed. To avoid reabsorption and inner filter effects, optical density was set to lower than 0.1 when measuring fluorescence spectra. All measurements were performed in a quartz cuvette with a 1 cm optical path at ambient temperature (25 \pm 2 °C). Full width at half maximum (FWHM) contours of the fluorescence were obtained by sectioning fluorescence spectra at all

excitation wavelengths according to a procedure schematically presented in Figure S2 of the Supporting Information.

2.6. Fourier Transformed Infrared (FTIR) Spectroscopy.

Analysis by infrared (IR) spectroscopy was carried out on a Vertex 70 FTIR spectrometer (Bruker Optik GmbH) with a GladiATR attenuated total reflection (ATR) attachment with a diamond crystal (Pike Technologies). The spectra recording range was 4000–350 cm^{-1} ; the resolution was 2 cm^{-1} ; and the number of scans was 64. To register the IR spectrum, 1 mg of a sample powder was dissolved in 10 μL of methanol and then about 1 μL was placed on an ATR crystal and dried. The data were collected and processed by OPUS version 7.5 software (Bruker). The bands were assigned according to the corresponding literature.³⁰

3. RESULTS

3.1. Sequential Solid-Phase Extraction (SPE) Separation of the Leonardite Humic Material, Followed by FTICR MS Analysis. The sample was separated into four fractions with the use of sequential SPE PPL extraction by a stepwise lowering of the pH value of the discharged solution. We adjusted the pH values to 7, 5, 3, and 2, taking into consideration a decrease in pK_a values of the acidic groups in the following sequence: phenols ($\text{pK}_a > 7$), unconjugated carboxylic acids ($\text{pK}_a \sim 5–4$), benzoic acids ($\text{pK}_a > 3$), and β -keto carboxylic acids or polycarboxylic acids ($\text{pK}_a < 2.5$).³¹ The overall extraction yield was 47%. The maximum yield was obtained at pH 7, which is drastically different from DOM, with the recommended extraction at pH 2³² (Figure S1 of the

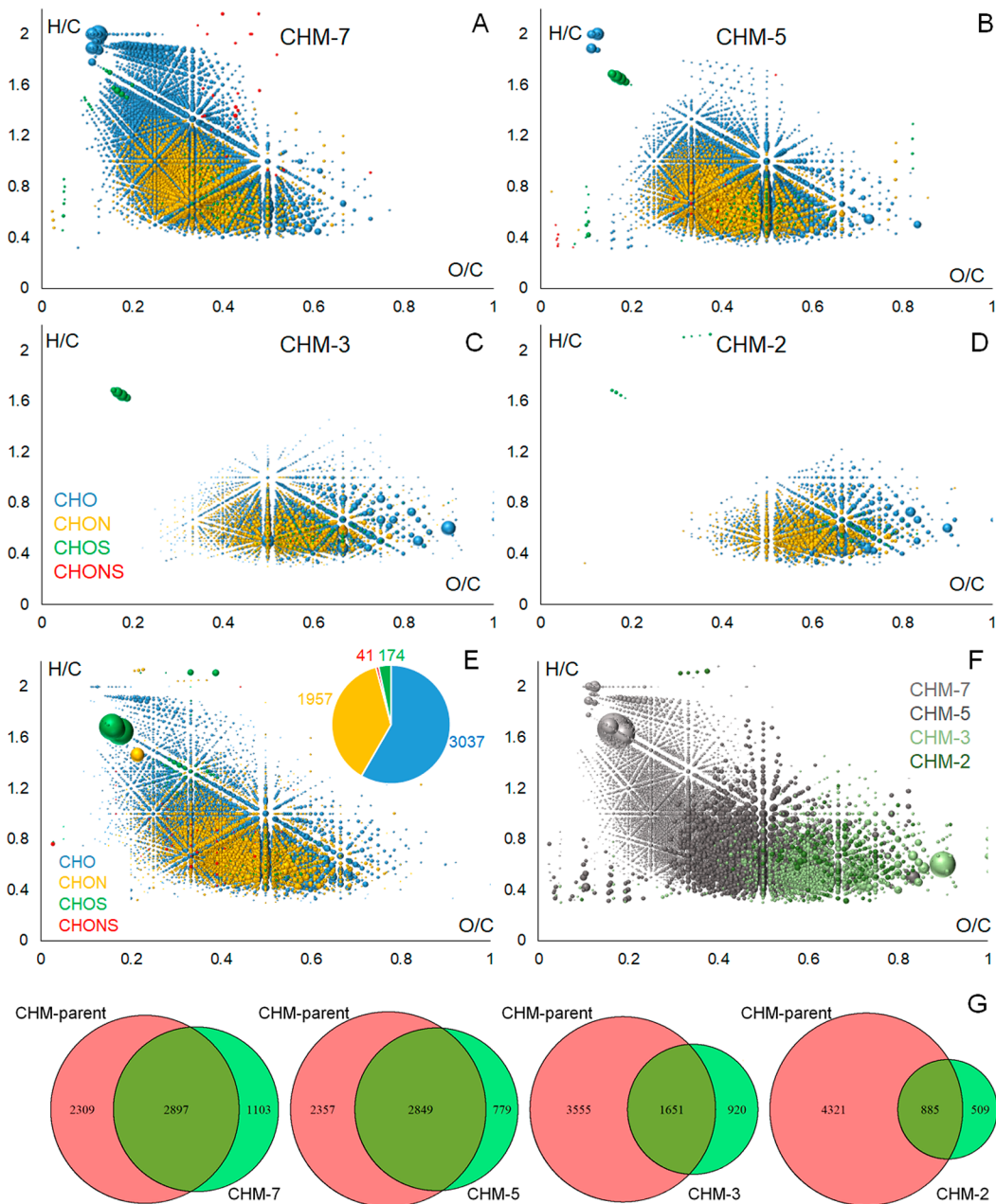


Figure 2. Van Krevelen diagrams plotted from the formula assignments made for the FTICR MS data for the (A–D) CHM fractions isolated using sequential SPE PPL extraction at different pH values, (E) original sample, and (F) combined fractions and (G) Venn diagrams for the native CHM sample and its four fractions.

Supporting Information). The obtained results are in agreement with our previous findings on the higher content of the carboxyl-depleted components in the case of leonardite HS compared to DOM.²¹

The FTICR mass spectra of the CHM fractions are presented in Figure 1. It can be seen that SPE fractionation led to only slight changes in the mass range; however, the number-averaged molecular mass (M_n) as well as the value of total peak intensity (TPI) depended upon pH: M_n and TPI decreased with a drop in pH from 438 Da and $23 \text{ TPI} \times 10^9$ to 406 Da and $12 \text{ TPI} \times 10^9$ for CHM-7 and CHM-2, respectively. This is in accordance with the previous findings that the most oxygenated compounds are of low molecular weight.³³ A decrease in the TPI value can be explained by the

poorer ionization efficiency of the most hydrophilic species by ESI compared to ionization of hydrophobic molecules.³⁴

Fine structures of the FTICR mass spectra revealed clear differences between the isolated fractions. The insets in Figure 1 present the magnified mass spectra plots corresponding to the value of nominal m/z of 359 for all CHM fractions. It can be seen that the reduced saturated molecules with the highest positive mass defect³⁵ accounted for maximum relative intensity in the case of CHM-7, e.g., $\text{C}_{20}\text{H}_{23}\text{O}_6$ and $\text{C}_{21}\text{H}_{21}\text{O}_5$ lignin-like components.³⁶ Along with a decrease in pH, the peak distribution progressively shifts toward aromatic oxidized molecules with the smaller mass defect, e.g., $\text{C}_{16}\text{H}_7\text{O}_{10}$ and $\text{C}_{14}\text{H}_9\text{O}_{11}$, which can be assigned to strong polycarboxylic acids.³⁷ Detailed representation of the evolution of oxygen classes and other heteroatoms within the humic molecular

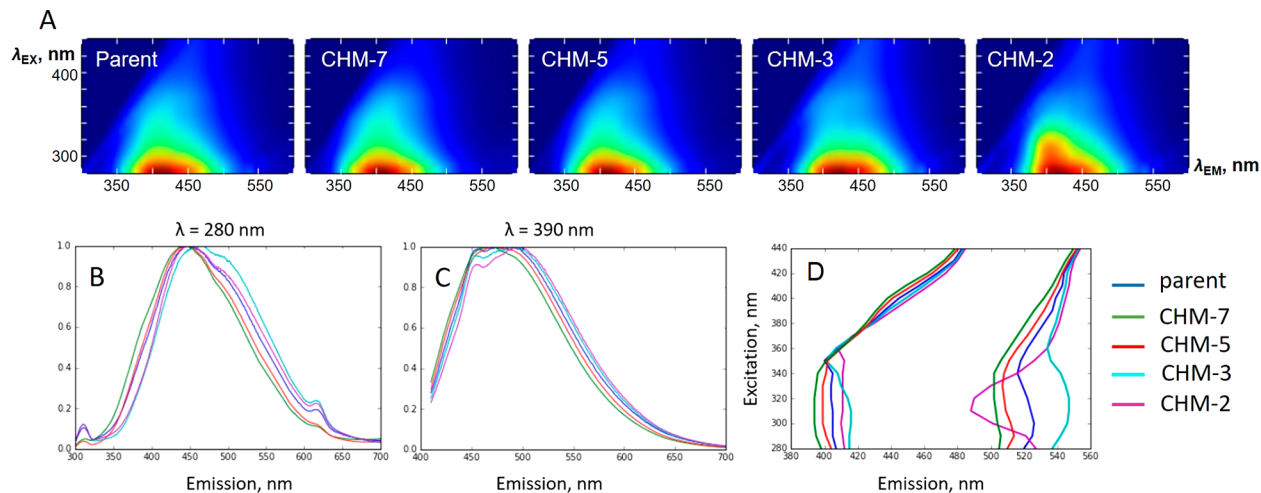


Figure 3. (A) EEMs, (B and C) fluorescence emission spectra at 280 and 390 nm excitation, respectively, and (D) fwhm contours for the parent CHM sample and its fractions at different excitation wavelengths.

ensemble of the pH fractions is given in Figure S3 of the Supporting Information. Overall, the data obtained are indicative of the efficient separation of the reduced and oxidized humic components on the PPL cartridge.

Evolution of the molecular space of the isolated fractions was visualized using the Van Krevelen diagrams (panels A–D of Figure 2). The pH series is characterized by a gradual shift in intensity from the relatively reduced saturated compounds with H/C > 1, which dominated in the CHM-7 sample, toward the highly unsaturated oxidized molecules with O/C > 0.6, which prevailed in the CHM-2 fraction. Previously, we identified the majority of lignin-like molecules present in the CHM-7 fraction as polyphenols without carboxylic substitutions.²¹ At the same time, the CHM-5 fraction was composed of lignin molecules containing oxidized primary alcohol³⁸ and CRAM molecules³⁹ with pK_a of unconjugated carboxylic acid. The molecular species in CHM-3 with H/C < 1 and O/C > 0.5 could be attributed to aromatic acids and tannins. The molecular population in Van Krevelen diagrams observed for CHM-2 could be readily attributed to ketoacids as a result of the highest value of the O/C ratio.

3.2. Fluorescence Spectroscopy. The trends observed in molecular compositions of the CHM fractions could potentially influence their optical properties. Figure S4 of the Supporting Information demonstrates the clear trend in intensity-weighted distribution of the aromaticity index (AI)⁴⁰ for all samples and their common formulas. Along with a decrease in pH, the AI distributions shifted toward the higher values. For instance, the portion of aromatic (AI > 0.5) and condensed (AI > 0.67) molecules in CHM-7 reached 23 and 69%, respectively, while for CHM-2, the corresponding values accounted for 57 and 86% (Table S1 of the Supporting Information).

Generally, an increase in the content of condensed aromatic moieties should lead to an increase in the red shift of HS optical (fluorescence and absorption) spectra; this suggestion was verified by measuring the fluorescence properties of the CHM fractions. Figure 3A demonstrates EEMs for all HS samples that exhibit a typical humic-like pattern.⁴¹ For $\lambda_{\text{ex}} > 370$ nm, we observed a gradual shift of emission parameters along a decrease in pH (Figure 3C), nominally, the red shift of fluorescence spectra, which could indicate an increase in the effective conjugation length and aromaticity of the sample.⁴²

This is also in agreement with the FTICR MS data. However, anomalous behavior was observed for the CHM-2 sample at $\lambda_{\text{ex}} \sim 280$ nm (Figure 3B). Although this sample was characterized by the highest portion of aromatic and condensed aromatic molecules (Table S1 of the Supporting Information), its fluorescence emission was less red-shifted in comparison to CHM-3. This phenomenon was visualized in Figure 3D, where the fwhm contours of the fluorescence emission spectra are presented for different excitation wavelengths. The following trend in the red shift was observed for $\lambda_{\text{ex}} < 350$ nm: CHM-7 < CHM-5 < native CHM < CHM-3. At the same time, the dependence of fwhm upon the excitation wavelength for CHM-2 was strongly non-monotonous. For $\lambda_{\text{ex}} > 350$ nm, the behavior of CHM-2 fluorescence followed the expected trend: CHM-7 < CHM-5 < native CHM < CHM-3 < CHM-2. The anomalous properties of CHM-2 are not characteristic for HS fluorescence and can be possibly explained by the dominant contribution of highly oxidized species and a lack of reduced unsaturated compounds, which is not typical of NOM.

3.3. One- and Two-Dimensional NMR and FTIR Spectroscopy. IR spectra for CHM-7, CHM-5, and CHM-2 are presented in Figure S5 of the Supporting Information. All samples display broad signals of water absorption in the region of 3680–3000 cm^{-1} . The main peaks corresponded to asymmetric and symmetric C–H stretching of aliphatic chains (2925 cm^{-1} with a 2850 cm^{-1} shoulder), C=O bond in carbonyl and carboxyl of amide groups (1710 cm^{-1}), aromatic C=C skeletal vibrations (1656 cm^{-1}), phenolic O–H deformation (1438 cm^{-1}), and C–O stretching in the carboxyl group (1242 cm^{-1}).³⁰ The intensity of the 2918 cm^{-1} band decreases with a drop in pH. Peaks attributed to C=O (1712 cm^{-1}) and C–O (1242 cm^{-1}) stretching in carboxylic groups were present in all spectra. However, in the case of CHM-7, these bands possess the lowest intensities, which indicate a lack of carboxylic groups in this fraction. Moreover, the proportion of carboxylic C–O and C=O to C–H band increases with the drop of pH.

To obtain the additional confirmation of separation efficiency of aromatic and aliphatic structural moieties revealed by FTICR MS and fluorescence spectroscopy, we performed ¹³C NMR analysis of all CHM fractions (Figure S6 of the Supporting Information). To perform quantitative analysis, we applied previously reported acquisition parameters.⁴³ The

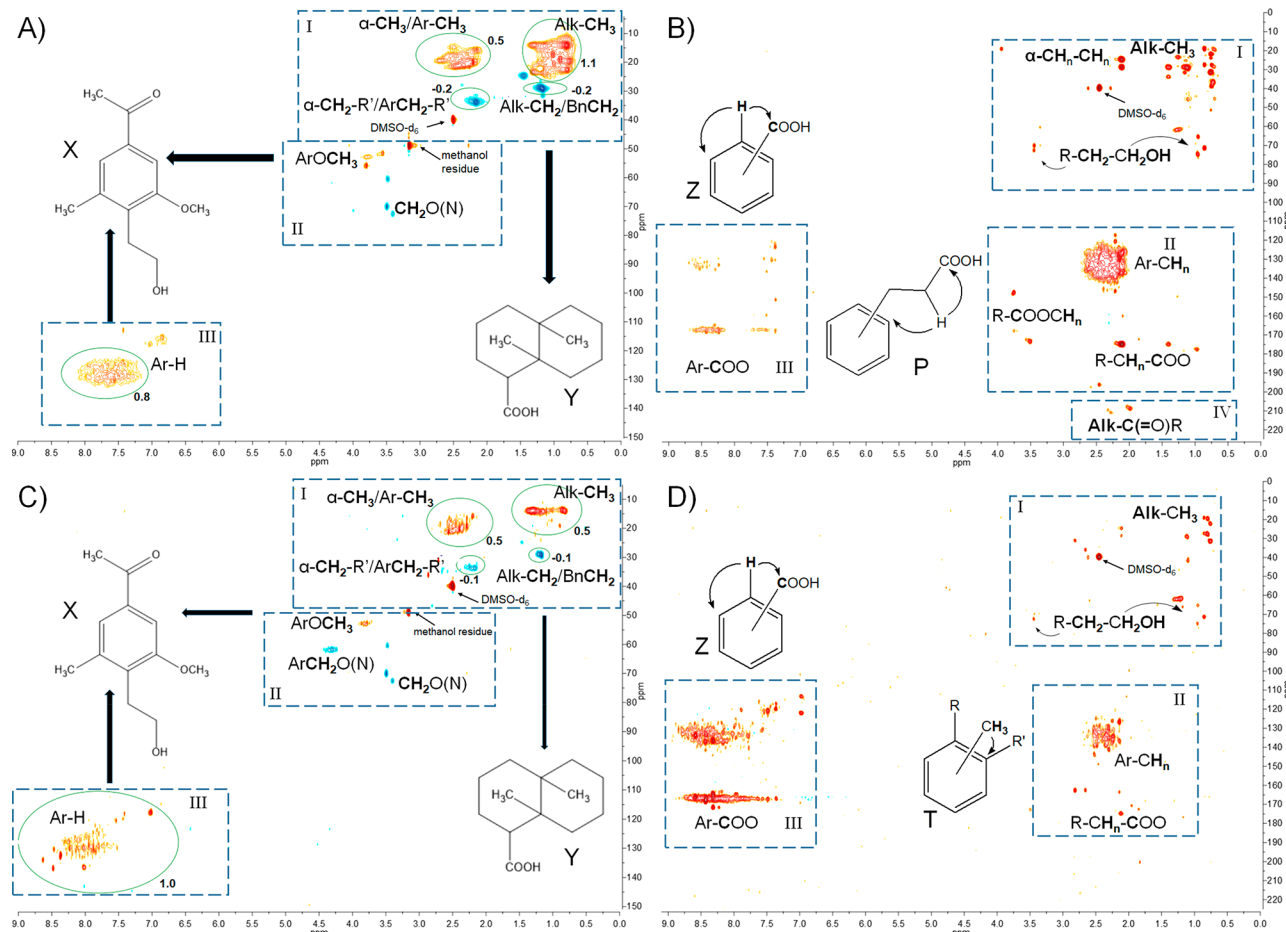


Figure 4. gHSQC and gHMBC NMR spectra of the CHM fractions obtained in this study: (A and B) CHM-5 and (C and D) CHM-3. Regions I, II, and III indicate the typical $^1\text{J}_{\text{CH}}$ and $^{2,3}\text{J}_{\text{CH}}$ cross peaks suggested for HS.⁵⁰

structural group compositions of the parent CHM material and its fractions are presented in Table 1. Along with a pH decrease, the contents of COO and carbonyl fragments in the corresponding fractions increased, indicating enrichment with acidic groups. At the same time, the CHM-7 sample was characterized with the highest relative contribution of aliphatic moieties (24%) compared to the bulk sample (15%) and other fractions (16 and 13% for CHM-5 and both CHM-3 and CHM-2, respectively). This could explain the largest yield of this fraction, which could result from the preferential affinity of the PPL resin for aliphatic species.⁴⁴ For a deeper investigation of the changes in structural motives of the obtained fractions, we employed correlation NMR spectroscopy for two fractions, CHM-5 and CHM-3, which were to contain carboxylic functionalities within different carriers: aliphatic and aromatic, respectively.

HSQC spectroscopy requires prior acquisition of one-dimensional (1D) spectra. The obtained ^1H NMR spectra of the CHM-5 and CHM-3 fractions as well as the results of their integration are presented in Figure S7 of the Supporting Information. CHM-5 was characterized by the maximum integral intensity of aliphatic protons (28%) with a $\text{CH}_n/\text{C}_{\text{ar}}\text{H}$ ratio of 1.2. The dominant integral intensity in the case of CHM-3 was assigned to aromatic protons (46%) with a $\text{CH}_n/\text{C}_{\text{ar}}\text{H}$ ratio of 0.3. This is indicative of enrichment in aromatic fragments caused by a drop of pH.

The HSQC spectra reveal a correlation between directly bonded C and H atoms in three major regions of the chemical shift (δ , ppm): aliphatic (δ_{H} from 0.5 up to 3.4 ppm and δ_{C} up to 45 ppm), heteroatom-substituted aliphatics (δ_{H} up to 5.6 ppm and δ_{C} up to 107 ppm), and aromatic systems (δ_{H} up to 9 ppm and δ_{C} up to 150 ppm).⁴³ The obtained HSQC spectra for CHM-5 and CHM-3 are presented in panels A and C of Figure 4. $^1\text{H}-^{13}\text{C}$ HSQC data show that the less acidic fraction (CHM-5) is characterized by intense cross peaks of $\text{C}^{sp^3}\text{H}_n$, indicating the dominant contribution of aliphatic moieties over aromatic moieties. Moreover, the intense cross peak in the strong field indicates contribution of methylene chains with terminal CH_3 groups, typical for terpenoids and fatty acids⁴⁵ (Figure 4A). A cross peak in the singly substituted aliphatic region might be assigned to methoxy groups typical for lignin. For CHM-3, on the contrary, the dominant correlation of aromatic carbon with protons was observed. This might be indicative of the abundance of low substituted aromatic moieties in this sample. The model structures, which could be responsible for the observed cross peaks of the CHM fractions, are presented in panels A and C of Figure 4. The predicted correlation spectra show similar cross peaks (Figure S8 of the Supporting Information).

HMBC experiments demonstrate long-range $^1\text{H}-^{13}\text{C}$ connectivities (generally up to three bonds) and provide information about specific structural fragments. Figure 4B shows a cross peak of aliphatic protons with carboxylic

moieties ($\delta_{\text{C}} > 170$ ppm), which indicates the aliphatic character of these carboxylic moieties. However, on the contrary to the riverine DOM, where only alicyclic, non-aromatic rings were seen in the HMBC spectrum,⁴⁶ we observed a correlation of the same protons with carboxylic, aliphatic (<50 ppm), and aromatic (110–150 ppm) carbons. This might be assigned to a three bond correlation, which indicates the presence of phenylpropanoic acids matching the predicted spectrum (Figure S8D of the Supporting Information). The obtained data demonstrate a substantial contribution of lignin-like structures into the CHM-5 fraction, which is in agreement with the HSQC results. The CHM-3 fraction was depleted in aliphatic carboxyls: we observed correlation of only aromatic protons with COOH moieties (Figure 4D). These aromatic protons were also connected to aromatic carbon. In comparison to CHM-5, we did not observe a two-bond correlation of aliphatic ^1H and ^{13}C in CHM-3. In agreement with the HSQC experiment, this fraction lacked hydrocarbon chains.

4. DISCUSSION

The conducted study shows that sequential pH gradient adsorption on SPE PPL enabled separation of the hymatomelanic acid from leonardite into four distinct fractions. The parent sample occupied a wide area on the Van Krevelen diagram (Figure 2E) from lipids to tannins,²⁸ which is typical for leonardite HS.⁴⁷ The combined fractions reproduced, in general, the molecular composition of parent CHM (Figure 2F). Despite a clear shift in molecular composition, some formulas were found within different fractions, e.g., $\text{C}_{16}\text{H}_7\text{O}_{10}$, shown in Figure 1. The appearance of the corresponding ion, even in mass spectra of quite different samples (CHM-7 and CHM-2), might indicate the separation of structural isomers presented in the parent sample. The isomeric complexity of HS was also suggested on the basis of the presence of the common ions in the mass spectra of HPLC fractions.²⁰

Contribution of the molecular constituents observed in the obtained fractions in the parent CHM sample is visualized in Figure 2G. Venn diagrams show that CHM-7 and CHM-5 comprise more than 50% of the molecular species identified in the parent sample. Moreover, the CHM-5 sample shows the smallest contribution of unique formulas compared to the other fractions. This is in line with the ^{13}C NMR data (Table 1), which reveal a similar content of aliphatic and aromatic moieties in the parent and CHM-5 samples. Along with a decrease in the pH value, a drop in the amount of the common formulas was observed in the parent CHM sample. This can be explained by enrichment of the fractions with the oxidized species, which possess a lower ionization efficiency compared to the reduced compounds.³⁴ As a result, parent CHM was depleted with highly oxidized components ($\text{O/C} > 0.8$), while they were abundant in CHM-3 and CHM-2 molecular compositions (Figure 2F). The NMR results also confirmed a change in the major type of carboxylic moieties along with a decrease in pK_a and a shift of dominant fragments from mostly aliphatic to almost exclusively aromatic moieties. ^{13}C NMR (Table S1 of the Supporting Information) reveals the maximum integral of carbonyl carbon in the CHM-2 fraction compared to the other fractions. In combination with FTICR MS results, this is a strong indication of the predominance of ketoacids in the CHM-2 fraction. The obtained data are in line with the findings of Leenheer et al.,⁴⁸ who attributed the major

acidic components in the riverine NOM to polycarboxylic acids with $\text{pK}_a < 2.5$. However, their presence in the coal sample has not been demonstrated thus far. Likely, further lowering the pH value would result in isolation of the most polar fraction of leonardite CHM. To support this idea, we analyzed permeate after extraction at pH 2 by IR spectroscopy (Figure S5 of the Supporting Information). We observe only a weak band of C–H stretching at 2925 cm^{-1} corresponding to aliphatic chains and a strong band of C–OH in the carboxylic group at 1242 cm^{-1} . Therefore, the structure of the non-retained fraction was depleted with aliphatic fragments.

Collectively, the results of this study indicate achievement of deep fractionation of the parent leonardite humic material. Moreover, pH control of stepwise extraction facilitated separation of aliphatic and aromatic units as well as the corresponding carboxylic carriers. This could be of particular importance for the study of metal–HS complexes. A previous investigation of a series of humic materials with different acidities, elemental compositions, and aromatic/aliphatic carbon ratios raised a question on the impact of functional groups and their type of carriers on complexation capacity.⁴⁹ Therefore, application of the proposed approach to commercial humic materials can be used to study the connection between molecular composition and major characteristics of the iron–HS complexes, such as stability or bioavailability. Further studies might enable design of iron-based fertilizers with better nutritional properties.

■ ASSOCIATED CONTENT

S Supporting Information

The Supporting Information is available free of charge on the ACS Publications website at DOI: [10.1021/acs.jafc.8b04079](https://doi.org/10.1021/acs.jafc.8b04079).

Additional information on the fluorescence spectroscopy, 1D NMR spectroscopy, and detailed consideration of the evolution of oxygen classes and other heteroatoms within the molecular ensemble of the pH fractions of the humic materials under study (PDF)

■ AUTHOR INFORMATION

Corresponding Authors

*Fax: +7-495-939-5546. E-mail: iperm@med.chem.msu.ru.

*E-mail: e.nikolaev@skoltech.ru.

ORCID

Alexander Zhrebker: [0000-0002-3481-4606](https://orcid.org/0000-0002-3481-4606)

Yury Kostyukevich: [0000-0002-1955-9336](https://orcid.org/0000-0002-1955-9336)

Irina V. Perminova: [0000-0001-9084-7851](https://orcid.org/0000-0001-9084-7851)

Author Contributions

Alexander Zhrebker was responsible for fractionation, data treatment, and manuscript preparation. Evgeny Shirshin was responsible for fluorescence measurements. Oleg Kharybin and Yury Kostyukevich were responsible for mass spectrometric analysis. Alexey Kononikhin was responsible for data interpretation and manuscript preparation. Andrey I. Konstantinov was responsible for quantitative ^{13}C NMR spectroscopy. Dmitry Volkov was responsible for IR spectroscopy. Vitaliy A. Roznyatovsky and Yuri K. Grishin were responsible for two-dimensional NMR spectroscopy and data interpretation. Irina V. Perminova and Eugene Nikolaev were responsible for supervision of the study and manuscript preparation.

Funding

This work was partially supported by the Russian Foundation for Basic Research (Grant 16-04-01753-a). Sample treatment was funded by the Russian Science Foundation (Grant 16-14-00167), and the high-resolution mass spectrometry study was funded by Russian Science Foundation Grant 18-79-10127. Correlation NMR experiments were supported by the Lomonosov Moscow State University "Program of Development". Optical measurements were supported by the Young Investigator Research Grant from the International Humic Substances Society.

Notes

The authors declare no competing financial interest.

ABBREVIATION USED

AI, aromaticity index; CHM, leonardite hymatomelanic acid; DOM, dissolved organic matter; EEM, excitation–emission matrix; ESI, electrospray ionization; FTICR MS, Fourier transform ion cyclotron resonance mass spectrometry; FTIR, Fourier transform infrared; fwhm, full width at half maximum; HILIC, hydrophilic interaction chromatography; HMBC, heteronuclear multiple bond correlation; HPLC, high-performance liquid chromatography; HS, humic substances; HSQC, heteronuclear single quantum coherence; IHSS, International Humic Substances Society; NOM, natural organic matter; NMR, nuclear magnetic resonance; SRFA, Suwannee River fulvic acid; SPE, solid-phase extraction; TPI, total peak intensity

REFERENCES

- (1) Swift, R. S. Organic Matter Characterization. In *Methods of Soil Analysis. Part 3. Chemical Methods*; Sparks, D. L., Page, A. L., Helmke, P. A., Loepert, R. H., Eds.; Soil Science Society of America (SSSA): Madison, WI, 1996; SSSA Book Series 5, Chapter 35, pp 1011–1069, DOI: 10.2136/sssabookser5.3.c35.
- (2) Nebbioso, A.; Piccolo, A. Basis of a Humeomics Science: Chemical Fractionation and Molecular Characterization of Humic Biosuprastructures. *Biomacromolecules* **2011**, *12* (4), 1187–1199.
- (3) Piccolo, A. The Supramolecular Structure of Humic Substances. *Soil Sci.* **2001**, *166* (11), 810–832.
- (4) Perminova, I. V.; Grechishcheva, N. Y.; Petrosyan, V. S. Relationships between Structure and Binding Affinity of Humic Substances for Polycyclic Aromatic Hydrocarbons: Relevance of Molecular Descriptors. *Environ. Sci. Technol.* **1999**, *33* (21), 3781–3787.
- (5) Villén, M.; Lucena, J. J.; Cartagena, M. C.; Bravo, R.; García-Mina, J.; De La Hinojosa, M. I. M. Comparison of Two Analytical Methods for the Evaluation of the Complexed Metal in Fertilizers and the Complexing Capacity of Complexing Agents. *J. Agric. Food Chem.* **2007**, *55* (14), 5746–5753.
- (6) Kovács, K.; Czech, V.; Fodor, F.; Solti, A.; Lucena, J. J.; Santos-Rosell, S.; Hernández-Apaolaza, L. Characterization of Fe-Leonardite Complexes as Novel Natural Iron Fertilizers. *J. Agric. Food Chem.* **2013**, *61* (50), 12200–12210.
- (7) Kulikova, N. A.; Polyakov, A. Y.; Lebedev, V. A.; Abroskin, D. P.; Volkov, D. S.; Pankratov, D. A.; Klein, O. I.; Senik, S. V.; Sorkina, T. A.; Garshev, A. V.; et al. Key Roles of Size and Crystallinity of Nanosized Iron Hydr(Oxides) Stabilized by Humic Substances in Iron Bioavailability to Plants. *J. Agric. Food Chem.* **2017**, *65* (51), 11157–11169.
- (8) Spaccini, R.; Piccolo, A. Molecular Characterization of Compost at Increasing Stages of Maturity. 1. Chemical Fractionation and Infrared Spectroscopy. *J. Agric. Food Chem.* **2007**, *55* (6), 2293–2302.
- (9) Piccolo, A.; Spaccini, R.; Drosos, M.; Vinci, G.; Cozzolino, V. The Molecular Composition of Humus Carbon: Recalcitrance and Reactivity in Soils. In *The Future of Soil Carbon*; Garcia, C., Nannipieri, P., Hernandez, T., Eds.; Elsevier, Cambridge, MA, 2018; Chapter 4, pp 87–124, DOI: 10.1016/B978-0-12-811687-6.00004-3.
- (10) Baigorri, R.; Zamarreño, A. M.; Fuentes, M.; González-Gaitano, G.; García-Mina, J. M.; Almendros, G.; González-Vila, F. J. Multivariate Statistical Analysis of Mass Spectra as a Tool for the Classification of the Main Humic Substances According to Their Structural and Conformational Features. *J. Agric. Food Chem.* **2008**, *56* (14), 5480–5487.
- (11) Baigorri, R.; Fuentes, M.; González-Gaitano, G.; García-Mina, J. M.; Almendros, G.; González-Vila, F. J. Complementary Multi-analytical Approach to Study the Distinctive Structural Features of the Main Humic Fractions in Solution: Gray Humic Acid, Brown Humic Acid, and Fulvic Acid. *J. Agric. Food Chem.* **2009**, *57* (8), 3266–3272.
- (12) Guo, A.; Wei, Z.; Zhao, B.; Chen, K.; Liu, D.; Wang, Z.; Song, H. Separation of Toluene-Insoluble Solids in the Slurry Oil from a Residual Fluidized Catalytic Cracking Unit: Determination of the Solid Content and Sequential Selective Separation of Solid Components. *Energy Fuels* **2014**, *28* (5), 3053–3065.
- (13) Aiken, G.; McKnight, D. M.; Thorn, K. A.; Thurman, E. M. Isolation of Hydrophilic Organic Acids from Water Using Nonionic Macroporous Resins. *Org. Geochem.* **1992**, *18* (4), 567–573.
- (14) Yonebayashi, K.; Hattori, T. A New Fractionation of Soil Humic Acids by Adsorption Chromatography. *Geoderma* **1990**, *47* (3–4), 327–336.
- (15) MacCarthy, P.; Peterson, M. J.; Malcolm, R. L.; Thurman, E. M. Separation of Humic Substances by PH Gradient Desorption from a Hydrophobic Resin. *Anal. Chem.* **1979**, *51* (12), 2041–2043.
- (16) Curtis, M. A.; Witt, A. F.; Schram, S. B.; Rogers, L. B. Humic Acid Fractionation, Using a Nearly Linear PH Gradient. *Anal. Chem.* **1981**, *53* (8), 1195–1199.
- (17) Hertkorn, N.; Ruecker, C.; Meringer, M.; Gugisch, R.; Frommberger, M.; Perdue, E. M.; Witt, M.; Schmitt-Kopplin, P. High-Precision Frequency Measurements: Indispensable Tools at the Core of the Molecular-Level Analysis of Complex Systems. *Anal. Bioanal. Chem.* **2007**, *389* (5), 1311–1327.
- (18) Sleighter, R. L.; Hatcher, P. G. The Application of Electrospray Ionization Coupled to Ultrahigh Resolution Mass Spectrometry for the Molecular Characterization of Natural Organic Matter. *J. Mass Spectrom.* **2007**, *42* (5), 559–574.
- (19) Woods, G. C.; Simpson, M. J.; Simpson, A. J. Oxidized Sterols as a Significant Component of Dissolved Organic Matter: Evidence from 2D HPLC in Combination with 2D and 3D NMR Spectroscopy. *Water Res.* **2012**, *46* (10), 3398–3408.
- (20) Stenson, A. C. Reversed-Phase Chromatography Fractionation Tailored to Mass Spectral Characterization of Humic Substances. *Environ. Sci. Technol.* **2008**, *42* (6), 2060–2065.
- (21) Zhrebker, A.; Kostyukevich, Y.; Kononikhin, A.; Kharybin, O.; Konstantinov, A. I.; Zaitsev, K. V.; Nikolaev, E.; Perminova, I. V. Enumeration of Carboxyl Groups Carried on Individual Components of Humic Systems Using Deuteromethylation and Fourier Transform Mass Spectrometry. *Anal. Bioanal. Chem.* **2017**, *409*, 2477–2488.
- (22) Kostyukevich, Y.; Acter, T.; Zhrebker, A.; Ahmed, A.; Kim, S.; Nikolaev, E. Hydrogen/Deuterium Exchange in Mass Spectrometry. *Mass Spectrom. Rev.* **2018**, *37*, 811–853.
- (23) Perminova, I. V. Analysis, Classification, and Prediction of Humic Acid Properties. Dr.Sc. Dissertation, Lomonosov Moscow State University, Moscow, Russia, 2000.
- (24) Dittmar, T.; Koch, B.; Hertkorn, N.; Kattner, G. A Simple and Efficient Method for the Solid-Phase Extraction of Dissolved Organic Matter (SPE-DOM) from Seawater. *Limnol. Oceanogr.: Methods* **2008**, *6*, 230–235.
- (25) Kostyukevich, Y. I.; Vladimirov, G. N.; Nikolaev, E. N. Dynamically Harmonized FT-ICR Cell with Specially Shaped Electrodes for Compensation of Inhomogeneity of the Magnetic Field. Computer Simulations of the Electric Field and Ion Motion Dynamics. *J. Am. Soc. Mass Spectrom.* **2012**, *23* (12), 2198–2207.
- (26) Zhrebker, A.; Turkova, A. V.; Kostyukevich, Y.; Kononikhin, A.; Zaitsev, K. V.; Popov, I. A.; Nikolaev, E.; Perminova, I. V.

- Synthesis of Carboxylated Styrene Polymer for Internal Calibration of Fourier Transform Ion Cyclotron Resonance Mass-Spectrometry of Humic Substances. *Eur. J. Mass Spectrom.* **2017**, *23* (4), 156–161.
- (27) Kunenkov, E. V.; Kononikhin, A. S.; Perminova, I. V.; Hertkorn, N.; Gaspar, A.; Schmitt-Kopplin, P.; Popov, I. A.; Garmash, A. V.; Nikolaev, E. N. Total Mass Difference Statistics Algorithm: A New Approach to Identification of High-Mass Building Blocks in Electrospray Ionization Fourier Transform Ion Cyclotron Mass Spectrometry Data of Natural Organic Matter. *Anal. Chem.* **2009**, *81* (24), 10106–10115.
- (28) Kim, S.; Kramer, R. W.; Hatcher, P. G. Graphical Method for Analysis of Ultrahigh-Resolution Broadband Mass Spectra of Natural Organic Matter, the van Krevelen Diagram. *Anal. Chem.* **2003**, *75* (20), 5336–5344.
- (29) Kovalevskii, D. V.; Permin, A. B.; Perminova, I. V.; Petrosyan, V. S. Conditions for Acquiring Quantitative ^{13}C NMR Spectra of Humic Substances. *Moscow Univ. Chem. Bull.* **2000**, *41*, 39–42.
- (30) Karpukhina, E.; Mikheev, I.; Perminova, I.; Volkov, D.; Proskurnin, M. Rapid Quantification of Humic Components in Concentrated Humate Fertilizer Solutions by FTIR Spectroscopy. *J. Soils Sediments* **2018**, 1–11.
- (31) Ragnar, M.; Lindgren, C. T.; Nilvebrant, N.-O. PKa-Values of Guaiacyl and Syringyl Phenols Related to Lignin. *J. Wood Chem. Technol.* **2000**, *20* (3), 277–305.
- (32) Li, Y.; Harir, M.; Lucio, M.; Kanawati, B.; Smirnov, K.; Flerus, R.; Koch, B. P.; Schmitt-Kopplin, P.; Hertkorn, N. Proposed Guidelines for Solid Phase Extraction of Suwannee River Dissolved Organic Matter. *Anal. Chem.* **2016**, *88* (13), 6680–6688.
- (33) Li, Y.; Harir, M.; Lucio, M.; Gonsior, M.; Koch, B. P.; Schmitt-Kopplin, P.; Hertkorn, N. Comprehensive Structure-Selective Characterization of Dissolved Organic Matter by Reducing Molecular Complexity and Increasing Analytical Dimensions. *Water Res.* **2016**, *106*, 477–487.
- (34) Nebbioso, A.; Piccolo, A.; Spiteller, M. Limitations of Electrospray Ionization in the Analysis of a Heterogeneous Mixture of Naturally Occurring Hydrophilic and Hydrophobic Compounds. *Rapid Commun. Mass Spectrom.* **2010**, *24* (21), 3163–3170.
- (35) Wu, Z.; Rodgers, R. P.; Marshall, A. G. Two- and Three-Dimensional van Krevelen Diagrams: A Graphical Analysis Complementary to the Kendrick Mass Plot for Sorting Elemental Compositions of Complex Organic Mixtures Based on Ultrahigh-Resolution Broadband Fourier Transform Ion Cyclotron Resonance. *Anal. Chem.* **2004**, *76* (9), 2511–2516.
- (36) Kujawinski, E. B.; Behn, M. D. Automated Analysis of Electrospray Ionization Fourier Transform Ion Cyclotron Resonance Mass Spectra of Natural Organic Matter. *Anal. Chem.* **2006**, *78* (13), 4363–4373.
- (37) Tfaily, M. M.; Hodgkins, S.; Podgorski, D. C.; Chanton, J. P.; Cooper, W. T. Comparison of Dialysis and Solid-Phase Extraction for Isolation and Concentration of Dissolved Organic Matter Prior to Fourier Transform Ion Cyclotron Resonance Mass Spectrometry. *Anal. Bioanal. Chem.* **2012**, *404* (2), 447–457.
- (38) Zhrebker, A. Y.; Airapetyan, D.; Konstantinov, A. I.; Kostyukevich, Y. I.; Kononikhin, A. S.; Popov, I. A.; Zaitsev, K. V.; Nikolaev, E. N.; Perminova, I. V. Synthesis of Model Humic Substances: A Mechanistic Study Using Controllable H/D Exchange and Fourier Transform Ion Cyclotron Resonance Mass Spectrometry. *Analyst* **2015**, *140* (13), 4708–4719.
- (39) Stubbins, A.; Spencer, R. G. M.; Chen, H.; Hatcher, P. G.; Mopper, K.; Hernes, P. J.; Mwamba, V. L.; Mangangu, A. M.; Wabakanganzi, J. N.; Six, J. Illuminated Darkness: Molecular Signatures of Congo River Dissolved Organic Matter and Its Photochemical Alteration as Revealed by Ultrahigh Precision Mass Spectrometry. *Limnol. Oceanogr.* **2010**, *55* (4), 1467–1477.
- (40) Kellerman, A. M.; Dittmar, T.; Kothawala, D. N.; Tranvik, L. J. Chemodiversity of Dissolved Organic Matter in Lakes Driven by Climate and Hydrology. *Nat. Commun.* **2014**, *5*, 3804.
- (41) Sierra, M. M. D.; Giovanel, M.; Parlanti, E.; Soriano-Sierra, E. J. Fluorescence Fingerprint of Fulvic and Humic Acids from Varied Origins as Viewed by Single-Scan and Excitation/Emission Matrix Techniques. *Chemosphere* **2005**, *58* (6), 715–733.
- (42) Boyle, E. S.; Guerriero, N.; Thiallet, A.; Del Vecchio, R.; Blough, N. V. Optical Properties of Humic Substances and CDOM: Relation to Structure. *Environ. Sci. Technol.* **2009**, *43* (7), 2262–2268.
- (43) Hertkorn, N.; Permin, A.; Perminova, I.; Kovalevskii, D.; Yudov, M.; Petrosyan, V.; Kettrup, A. Comparative Analysis of Partial Structures of a Peat Humic and Fulvic Acid Using One- and Two-Dimensional Nuclear Magnetic Resonance Spectroscopy. *J. Environ. Qual.* **2002**, *31*, 375–387.
- (44) Perminova, I. V.; Dubinenkov, I. V.; Kononikhin, A. S.; Konstantinov, A. I.; Zhrebker, A. Y.; Andzhushhev, M. A.; Lebedev, V. A.; Bulygina, E.; Holmes, R. M.; Kostyukevich, Y. I.; et al. Molecular Mapping of Sorbent Selectivities with Respect to Isolation of Arctic Dissolved Organic Matter as Measured by Fourier Transform Mass Spectrometry. *Environ. Sci. Technol.* **2014**, *48* (13), 7461–7468.
- (45) Hertkorn, N.; Benner, R.; Frommberger, M.; Schmitt-Kopplin, P.; Witt, M.; Kaiser, K.; Kettrup, A.; Hedges, J. I. Characterization of a Major Refractory Component of Marine Dissolved Organic Matter. *Geochim. Cosmochim. Acta* **2006**, *70* (12), 2990–3010.
- (46) Lam, B.; Baer, A.; Alaee, M.; Lefebvre, B.; Moser, A.; Williams, A.; Simpson, A. J. Major Structural Components in Freshwater Dissolved Organic Matter. *Environ. Sci. Technol.* **2007**, *41* (24), 8240–8247.
- (47) Zhrebker, A. Y.; Kostyukevich, Y. I.; Kononikhin, A. S.; Nikolaev, E. N.; Perminova, I. V. Molecular Compositions of Humic Acids Extracted from Leonardite and Lignite as Determined by Fourier Transform Ion Cyclotron Resonance Mass Spectrometry. *Mendelev Commun.* **2016**, *26* (5), 446–448.
- (48) Leenheer, J. A.; Wershaw, R. L.; Reddy, M. M. Strong-Acid, Carboxyl-Group Structures in Fulvic Acid from the Suwannee River, Georgia. 2. Major Structures. *Environ. Sci. Technol.* **1995**, *29* (2), 399–405.
- (49) Fujii, M.; Imaoka, A.; Yoshimura, C.; Waite, T. D. Effects of molecular composition of natural organic matter on ferric iron complexation at circumneutral pH. *Environ. Sci. Technol.* **2014**, *48* (8), 4414–4424.
- (50) Hertkorn, N.; Harir, M.; Koch, B. P.; Michalke, B.; Schmitt-Kopplin, P. High-Field NMR Spectroscopy and FTICR Mass Spectrometry: Powerful Discovery Tools for the Molecular Level Characterization of Marine Dissolved Organic Matter. *Biogeosciences* **2013**, *10* (3), 1583–1624.